Sonar Propagation Modeling using Hybrid Gaussian Beams in Spherical/Time Coordinates

Sean M. Reilly

Department of Ocean Engineering, University of Rhode Island,
Narragansett RI, USA
campreilly@my.uri.edu

Gopu Potty

Department of Ocean Engineering, University of Rhode Island,
Narragansett RI, USA
potty@egr.uri.edu

Michael Goodrich

Alion Science and Tecnology Corporation,
Norfolk VA, USA
mgoodrich@alionscience.com

This paper [*] defines a new 3–D underwater acoustic propagation loss model that is specifically formulated to provide a significant speed advantage to real-time, active sonar, simulation/stimulation systems in littoral environments. The ray solutions to the eikonal equation are computed in latitude, longitude, and altitude coordinates to match wide-area environmental databases. Hybrid Gaussian beam techniques for propagation loss calculation are used to extend the applicability of ray theory to lower frequency regimes. Numerical integration of the wave equation is performed in the time dimension to maintain the phase continuity of the wavefront. This 3–D approach supports horizontal refraction and out-of-plane reflection from the ocean bottom. Computing the transmission loss in the same coordinate system as the environmental parameters should provide this model with a computational speed advantage over other models. The derivation of this new model requires the development of new equations for ray tracing, reflection, eigenray finding, and Gaussian beam propagation loss. This paper examines that derivation.

Keywords: Gaussian beams; 3–D modeling; range-dependent; time-domain.

1. Introduction

Ray models are one of the oldest techniques for understanding sound propagation in the ocean. Although much of the current literature focuses on full-wave methods, such as normal mode and parabolic equation, range-dependent ray theory is still used frequently by real-time sonar simulation/stimulation systems to compute propagation loss. This is partly due to the fact that ray models run quickly, and partly because they provide the travel time and

---

direction information needed for sonar stimulation. This preference is particularly acute at higher frequencies (above 1000 Hz), where full-wave methods become prohibitively slow. Unfortunately, ray models can also suffer from significant accuracy limitations: they predict perfect shadow zones in areas of the water column where rays do not propagate, and they predict infinite intensity at caustics, places where the ray paths cross.[1] These effects are not seen in nature and full-wave models do not suffer from these problems. Gaussian beams are an augmentation of ray theory that attempts to address these limitations while keeping many of ray theory's benefits. This paper builds on the prior art in Gaussian beam theory to create a new propagation loss model that operates in a fully 3–D environment. Future papers will focus on the verification, validation, and computational efficiency of this new model.

The Gaussian beam components of this new approach leverage the concepts developed by H. Weinberg et. al.[2,3] for the Gaussian Ray Bundling (GRAB) model. Gaussian beam models compute propagation loss by spreading the energy associated with each ray path, across the wavefront, out to a distance that is proportional to the divergence of the acoustic field along this path. The propagation loss for each target is computed by summing the contributions from many passing rays. This enhancement eliminates the tendency toward infinite intensity at caustics, and it produces penetration into shadow zones, especially at low frequencies.

In 1982, V. Červený et. al.[4] developed a rigorous method for computing seismic Gaussian beams. Červený's approach uses dynamic ray equations to compute the divergence of the field along the ray path. In 1987, M. B. Porter et. al.[5,6] extended this work to underwater acoustics and created the BELLHOP† model. GRAB (1996) leverages this prior work, but calculates the divergence using the distance between ray paths, much like classic ray theory. The fact that GRAB does not need to compute and maintain the dynamic ray equations, gives it a speed advantage over these other methods. In general, Gaussian beam propagation loss calculations are expected to be most accurate at frequencies above 1000 Hz, but GRAB has successfully used these techniques to support accurate results at frequencies as low as 150 Hz. Because GRAB combines Gaussian beams with traditional ray theory, it is sometimes categorized as a "hybrid" Gaussian beam model. All of these models are based on a Cartesian 2–D coordinate system and they use multiple radials to model 3–D effects. This process is often referred to as a 2–DxN approach.

The new algorithm uses geographic latitude, longitude, and altitude as the basis for a 3–D propagation environment. This approach is very similar to the one developed by R. M. Jones et. al.[7] for the Hamiltonian Ray-Tracing Program for the Ocean (HARPO). This coordinate system not only supports horizontal refraction, and out-of-plane reflection, but also allows ray tracing to be performed in the same coordinate system as environmental parameter databases. Most ray theory models, including all of the models referenced above, are based on solutions to the eikonal equation, the high frequency limit of Helmholtz equation. The HARPO model is unusual in that it solves the Hamilton equation, the differential

---

†BELLHOP is not an acronym.

expression of Fermat's principle, using an elliptical earth. This difference gives HARPO the ability to model the frequency spreading effects associated with ocean advection on planetary scales. However, at this time, HARPO only computes ray paths, not propagation loss.

This paper combines all of these concepts into a new propagation loss algorithm that is specifically formulated to provide a significant speed advantage to real-time, active sonar, simulation/stimulation systems in littoral environments. It solves the eikonal ray tracing equations as functions of geographic latitude, longitude, and altitude. The earth is modeled as a sphere, with a radius that depends on the area of operations, instead of using HARPO's elliptical representation, to simplify this computation, Although there are increased computational requirements for modeling Gaussian beams in this coordinate system, the impact on calculation speed is balanced by the ability to compute solutions without transforming environmental parameter databases into 2–DxN radials. Numerical integration of the ray equations is performed in the time dimension to maintain the phase continuity of the wavefront, which simplifies the eigenray finding geometry. Propagation loss is calculated using a technique that is similar to GRAB, but translated into a new 3–D coordinate system. The derivation of this new approach requires the development of new equations for ray tracing, reflection, eigenray finding, and Gaussian beam propagation loss. This paper examines that derivation.

2. Ray Tracing in Spherical/Time Coordinates

The ray tracing equations used by this model are

$$\frac{dr}{dt} = c^2 \alpha \, , \tag{1}$$

$$\frac{d\theta}{dt} = \frac{c^2 \beta}{r} \, , \tag{2}$$

$$\frac{d\phi}{dt} = \frac{c^2 \gamma}{r \sin\theta} \, , \tag{3}$$

$$\frac{d\alpha}{dt} = -\frac{1}{c}\frac{dc}{dr} + \frac{c^2}{r}\left(\beta^2 + \gamma^2\right) \, , \tag{4}$$

$$\frac{d\beta}{dt} = -\frac{1}{cr}\frac{dc}{d\theta} - \frac{c^2}{r}\left(\alpha\beta + \gamma^2 \cot\theta\right) \, . \tag{5}$$

$$\frac{d\gamma}{dt} = -\frac{1}{cr\sin\theta}\frac{dc}{d\phi} - \frac{c^2\gamma}{r}\left(\alpha + \beta\cot\theta\right) \, , \tag{6}$$

where c is the speed of sound in water; t is the travel time along the ray path; (r, θ, ϕ) are the spherical components of $\vec{r}$, the position along a ray path; and (α, β, γ) are the spherical components of $\vec{\xi}$, the propagation direction divided by the speed of sound. Equations (1) through (6) compute the time evolution for the location and direction for any acoustic ray based on its initial conditions. These equations are derived from first principles in Appendix A. These equations support 3–D refraction effects and incorporate earth curvature effects, including great circle routes between locations. Environmental parameters and their derivatives are computed directly in geographic latitude, longitude, and altitude without reducing the problem to a series of 2–DxN radials or a flat earth Cartesian projection.

This model uses an explicit, third order, Adams-Bashforth (AB3) algorithm[8] to propagate Eqs. (1) through (6) numerically. The AB3 algorithm, summarized in Eq. (7), approximates each step in the solution for f(t) using explicit information from the three time steps that came before it. Since these past values can be cached, AB3 is much faster than other methods with similar accuracy. However, because AB3 is not self-starting, this model uses a third order Runge-Kutta (RK3) algorithm[9] whenever the ray parameters must be initialized, or re-initialized

$$f(t_{n+1}) = f(t_n) + \delta t \left[\frac{23}{12} \frac{df}{dt}(t_n) - \frac{16}{12} \frac{df}{dt}(t_{n-1}) + \frac{5}{12} \frac{df}{dt}(t_{n-2}) \right] . \tag{7}$$

Even though Eqs. (1) through (6) look complex, the ray tracing is still expected to be more computationally efficient than an equivalent 2–DxN calculation in Cartesian coordinates. Most of these savings are a result of the fact that this model avoids transformation of the environmental inputs. These savings will be most significant in highly dynamic 3–D simulation environments where the re-use of pre-computed environments is not practical. It is helped by the fact that the interpolation of the speed of sound and its gradient, an expensive operation for gridded databases, have been limited to a single instance per iteration. In addition, the computationally expensive trigonometric calculations have been reduced to a single $sin\theta$ and $cot\theta$ factor per iteration.

3. Boundary Reflections on a Spherical Earth

The first step in modeling an interface reflection is estimating the point in time when the incident ray strikes the bottom. The derivation of the equations for estimating the time of reflection in spherical coordinates uses the symbols defined in Fig. 1 where $\vec{I}$ is the incident ray path; ζ is the incident grazing angle; $\hat{s}$ is the surface normal; $\hat{r}$ is the unit vector in the radial direction; h is the incident ray height above bottom; Δt is the normal time step; and δt is the time step needed to reach the interface. Note that, to simplify the geometry, Fig. 1 is drawn in the plane of reflection. Fig. 2 illustrates this same scenario in a 3-D perspective.

If the bottom slope is nearly constant across the length of the incident ray, then the ratio of the time steps is equivalent to the ratio of the distances normal to the surface

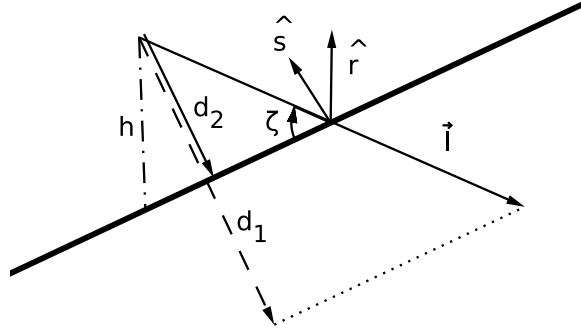$$d_1 \equiv -\vec{I} \cdot \hat{s} = - \left(\frac{d\vec{r}}{dt} \cdot \hat{s} \right) \Delta t , \tag{8}$$

Fig. 1. Estimating the point of reflection.

$$d_2 \equiv -h\hat{r} \cdot \hat{s} \,, \tag{9}$$

$$\frac{\delta t}{\Delta t} = \frac{d_2}{d_1} = \frac{h\,\hat{r} \cdot \hat{s}}{\left(\dfrac{d\vec{r}}{dt} \cdot \hat{s}\right)\Delta t} \,, \tag{10}$$

$$\delta t = \frac{h\,\hat{r} \cdot \hat{s}}{\dfrac{d\vec{r}}{dt} \cdot \hat{s}} \,. \tag{11}$$

At the ocean surface, this simplifies to

$$\delta t_{surface} = \frac{h}{\frac{dr}{dt}} \,, \tag{12}$$

where $\frac{dr}{dt}$ is the radial ray tracing component defined in Eq. (1). To improve the accuracy of the reflection geometry, the new model also applies a second order Taylor expansion to each component of the position, normalized direction, and sound speed, to find their values at the point defined by Eq. (10).

The next step in reflection modeling is estimating the direction of reflection from a 3–D slope. The derivation of the equations for estimating this direction in spherical coordinates uses the symbols defined in Fig. 2 where $\hat{I}$ is the incident ray path direction; $\hat{R}$ is the reflected ray path direction; and $\vec{B}$ is the component of the incident ray that is perpendicular to surface normal.

Since the reflected ray has the same angle to the normal as the incident ray

$$\hat{R} = 2\vec{B} - \hat{I} \,, \tag{13}$$

$$\vec{B} = \hat{I} - (\hat{I} \cdot \hat{s})\hat{s} \,, \tag{14}$$
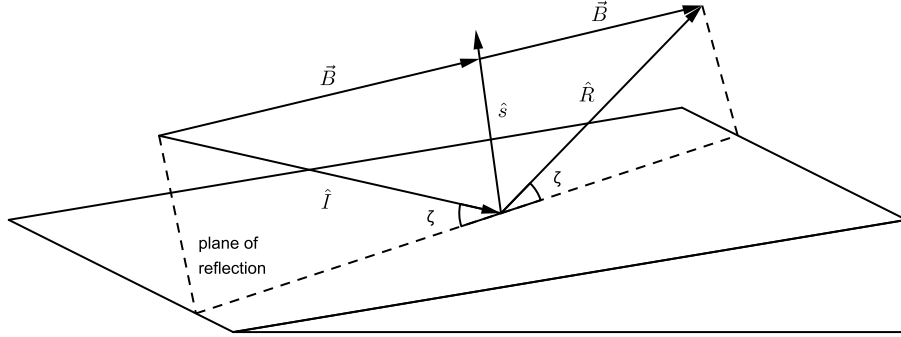
6   *S. M. Reilly, G. Potty*

Fig. 2. Reflection from a 3–D slope.

$$\hat{R} = \hat{I} - 2(\hat{I} \cdot \hat{s})\hat{s} \,. \tag{15}$$

For ocean surface reflections, these relationships negate the sign of the radial component while leaving the θ and ϕ direction components unchanged.

Most bottom depth databases grid the relief of the earth's surface into a series of geographic latitude and longitude points. The spherical components of the surface normal (s_r, s_θ, s_ϕ) are computed by equating the slope $(\sigma_\theta, \sigma_\phi)$ to the first derivative of b, the boundary altitude.

$$\Omega_\theta \equiv tan(\sigma_\theta) = \frac{1}{b}\frac{db}{d\theta} \,, \tag{16}$$

$$\Omega_\phi \equiv tan(\sigma_\phi) = \frac{1}{b\,sin\theta}\frac{db}{d\phi} \,, \tag{17}$$

$$s_\theta = -sin(\sigma_\theta) = -\frac{\Omega_\theta}{\sqrt{1+\Omega_\theta^2}} \,, \tag{18}$$

$$s_\phi = -sin(\sigma_\phi) = -\frac{\Omega_\phi}{\sqrt{1+\Omega_\phi^2}} \,, \tag{19}$$

$$s_r = \sqrt{1 - (s_\theta^2 + s_\phi^2)} \,. \tag{20}$$

After reflection, the ray must be reinitialized in a way that maintains the phase continuity of the wavefront. This model uses a third order Runge-Kutta (RK3) algorithm to reverse propagation from the point of reflection back to the t_n, t_{n-1}, t_{n-2} points in time, during reinitialization.
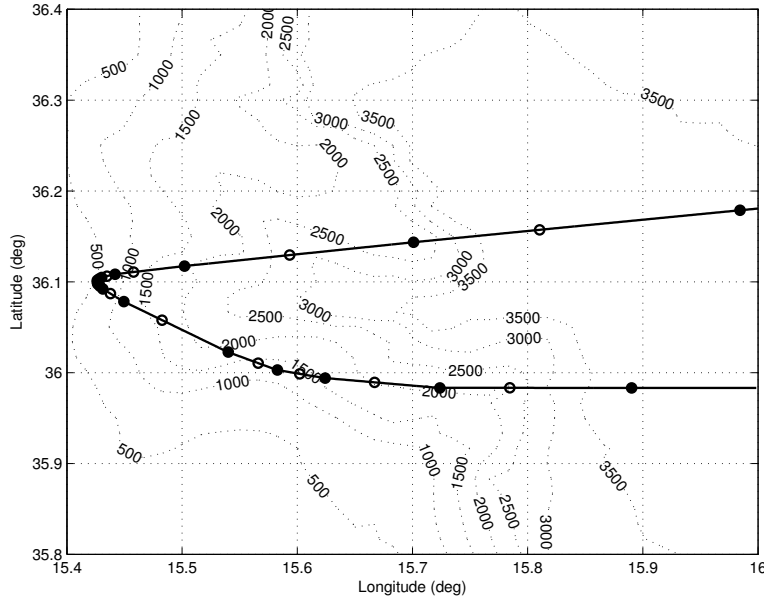
Fig. 3. 3-D Reflection on the Malta Escarpment.

ETOPO1 gridded bathymetry[10] from the Malta Escarpment was used to test out-of-plane reflection from real world bathymetry features. The results of this test are shown in Fig. 3. In this Fig., bottom bathymetry contours are represented as dashed lines. A ray is launched from 35:59N 16:00E, at a depth of 10 meters, with a depression/elevation angle of -20º (down), and an azimuth of 270º. The solid black line follows the trajectory of the ray as a function of latitude and longitude. The open circles along this path represent places where surface reflections occurred; the closed circles represent bottom reflections. The speed of sound was artificially fixed at 1500 m/s, and a time step of 100 ms was used to compute ray paths. The decrease in spacing between the shallow water dots illustrates an increase in the ray's depression/elevation angle as it reflects up the slope. In addition, ray paths were reflected into a new azimuthal direction each time that they interacted with the bottom. These out-of-plane reflections result in a down slope ray path that is offset by more than 21.9 km from the up slope path, after 14 bounces off of the bottom. This type of out of plane reflection is exactly the type of behaviors that we would expect from real-world bathymetry.[11]

4. Finding Eigenrays using Coherent Wavefronts

In this model, eigenrays are derived from each target's geometry relative to a Closest Point of Approach (CPA) on the wavefront. A point on the wavefront is the CPA for a specific target if the distance to that target is less than the same measurement in the twenty-six wavefront points that surround it. The coordinates for this distance calculation are illustrated in Fig. 4

8   *S. M. Reilly, G. Potty*

where $\vec{r}_p$ is the position of the eigenray target; $\vec{r}_{njk}$ is the position of the candidate points on the wavefront; d_{njk} is the distance from target to each point on wavefront; δt is the target offset along the direction of propagation; $\delta\mu$ is the target offset in the depression/elevation direction; and $\delta\varphi$ is the target offset in the azimuthal direction.
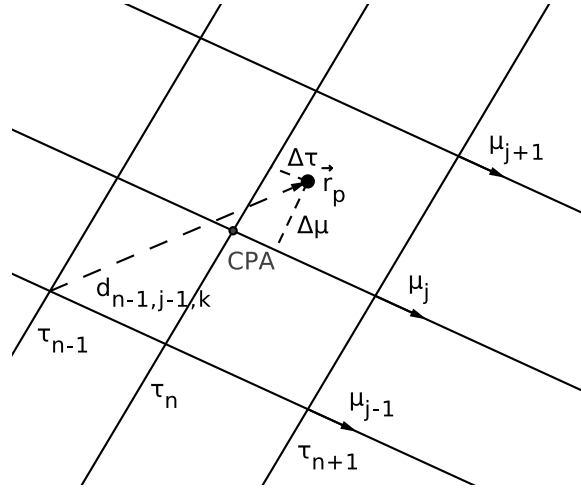

Fig. 4. Eigenray estimation geometry (side view: φ_k direction not shown).

An efficient calculation for the square of the distance in spherical coordinates can be derived from the Haversine formula[12]

$$d_{njk}^2 = r_p^2 + r_{njk}^2 - 2\vec{r}_p \cdot \vec{r}_{njk} \, , \tag{21}$$

$$d_{njk}^2 = r_p^2 + r_{njk}^2 - 2r_p r_{njk} \left[sin(\chi_p)sin(\chi_{ijk}) + cos(\chi_p)cos(\chi_{ijk})cos(\phi_p - \phi_{ijk}) \right] \, , \tag{22}$$

$$d_{njk}^2 = r_p^2 + r_{njk}^2 - 2r_p r_{njk} \left[1 - 2\left\{ sin^2\left(\frac{\chi_p - \chi_{ijk}}{2} \right) \right. \right.$$
$$\left. \left. + cos(\chi_p)cos(\chi_{ijk})sin^2\left(\frac{\phi_p - \phi_{ijk}}{2} \right) \right\} \right] \, , \tag{23}$$

$$d_{njk}^2 \approx r_p^2 + r_{njk}^2 - 2r_p r_{njk} \left[1 - 2\left\{ \left(\frac{\chi_p - \chi_{ijk}}{2} \right)^2 \right. \right.$$
$$\left. \left. + cos(\chi_p)cos(\chi_{ijk})\left(\frac{\phi_p - \phi_{ijk}}{2} \right)^2 \right\} \right] \, , \tag{24}$$

$$d_{njk}^2 \approx r_p^2 + r_{njk}^2 - 2r_p r_{njk} \left[1 - 2\left\{ \left(\frac{\theta_p - \theta_{ijk}}{2} \right)^2 + sin(\theta_p)sin(\theta_{ijk})\left(\frac{\phi_p - \phi_{ijk}}{2} \right)^2 \right\} \right] \, . \tag{25}$$

The accuracy of this approximation improves as the distance between the target and the wavefront decreases. If the implementation caches values for $sin\theta$ at both the wavefront and target locations, Eq. (25) allows d^2_{njk} to be computed without the use of any additional transcendental functions.

The offset of each target relative to the travel time (t), depression/elevation launch angle (μ), and the azimuthal launch angle (φ) coordinates of the CPA are needed to compute eigenrays. This model calculates these offsets by expressing d^2_p, the square of the distance at the target point, as a second order Taylor series, in vector form, relative to the CPA

$$\vec{\rho} \equiv (\rho_1, \rho_2, \rho_3) \equiv (\delta t, \delta\mu, \delta\varphi) , \tag{26}$$

$$d^2_p \approx \epsilon + \vec{g} \cdot \vec{\rho} + \frac{1}{2}\vec{\rho} \cdot \mathbf{H}\,\vec{\rho} , \tag{27}$$

$$\epsilon \equiv d^2\big|_{CPA} , \tag{28}$$

$$\vec{g} \equiv \frac{\partial d^2}{\partial \vec{\rho}}\big|_{CPA} , \tag{29}$$

$$\mathbf{H} \equiv \frac{\partial^2 d^2}{\partial \vec{\rho}^2}\big|_{CPA} \tag{30}$$

where $\vec{\rho}$ is the target offset from CPA in vector form; $\vec{g}$ is the gradient of squared distance at CPA (3 elements), and $\mathbf{H}$ is the Hessian matrix of squared distance at CPA (3x3).

One way to solve this equation would be to search for a value of $\vec{\rho}$ for which Eq. (27) was zero. However, since d^2_p is positive definite, the problem can be simplified by searching for the minimum value, indicated by a zero in the first derivative

$$\frac{\partial d^2_p}{\partial \vec{\rho}} = \vec{g} + \mathbf{H}\,\vec{\rho} = 0 , \tag{31}$$

$$\mathbf{H}\,\vec{\rho} = -\vec{g} , \tag{32}$$

$$\vec{\rho} = -\mathbf{H}^{-1}\,\vec{g} . \tag{33}$$

This treatment reduces the offset estimation problem to the calculation of the gradient of distance, the calculation of the Hessian matrix, and a matrix inversion. Note that the inverse of a 3x3 matrix has a simple analytic solution that allows it to be solved efficiently and without approximation.

Some eigenray products can be computed directly from this offset vector solution

$$t_p = t_n + \delta t , \tag{34}$$

$$\mu_p = \mu_j + \delta\mu , \tag{35}$$

$$\varphi_p = \varphi_k + \delta\varphi \tag{36}$$

where t_p is the travel time to the target; μ_p is the depression/elevation launch angle at source; and φ_p is the azimuthal launch angle at source. The direction at the target location is computed by forward solving the 2nd order Taylor series in the neighborhood of the CPA.

This eigenray detection process is less efficient than an equivalent calculation in Cartesian coordinates. However, the impact of this difference is minimized when the number of targets is small compared to the number ray tracing points; a good assumption for real-time, sonar simulation/stimulation systems. Unfortunately, this assumption may make this model inefficient for tactical decision aids, because the number of target points is large in those applications.

5. Computing Propagation Loss using 3–D Hybrid Gaussian Beams

In conventional ray theory, the acoustic spreading loss is estimated by measuring the changes in ensonified area between ray paths. The intensity across the wavefront is inversely proportional to the change in a surface area segment compared to its area at the source. The Červený approach uses dynamic ray equations to compute the divergence of the acoustic field normal to the path of propagation. The new model assumes that this divergence can be estimated from the wavefront shape directly, and that keeping all of the points co-temporal across the on the wavefront simplifies the geometry for this estimate. Like the GRAB model, this new approach only needs to calculate divergence during an eigenray encounter with a target. Unlike the GRAB model, neighboring contributions in the divergence are guaranteed to be in phase. This approach is computationally efficient when there are multiple eigenray targets for each source, but the total number of targets is small.

In all Gaussian beam models, the intensity at the target location is a summation of contributions from the rays that surround the eigenray target. To create a 3–D acoustic field across the wavefront, the new model uses independent Gaussian beams in the μ and φ directions and ignores the cross terms. As illustrated in Fig. 5 and Eq. (37), this assumption decomposes the Gaussian ray contributions to a series of nearest neighbor lines in the μ and φ directions

$$G(\vec{r}_p) = \left(\sum_{j'=j-J}^{j+J} g_{j'}(\vec{r}_p) \right) \left(\sum_{k'=k-K}^{k+K} g_{k'}(\vec{r}_p) \right), \tag{37}$$

where $G(\vec{r}_p)$ is the total Gaussian beam intensity at the eigenray target; (j, k) are the index numbers of cell containing the eigenray target; $g_{j'}$ are the Gaussian beam contributions along depression/elevation direction; $g_{k'}$ are the Gaussian beam contributions along the azimuthal direction; $2J + 1$ are the number of significant beams in the depression/elevation direction; and $2K + 1$ are the number of significant beams in the azimuthal direction.

The intensity of each Gaussian beam contribution is a function of the width of the beam and the distance along the wavefront to the eigenray target, normalized to the surface area
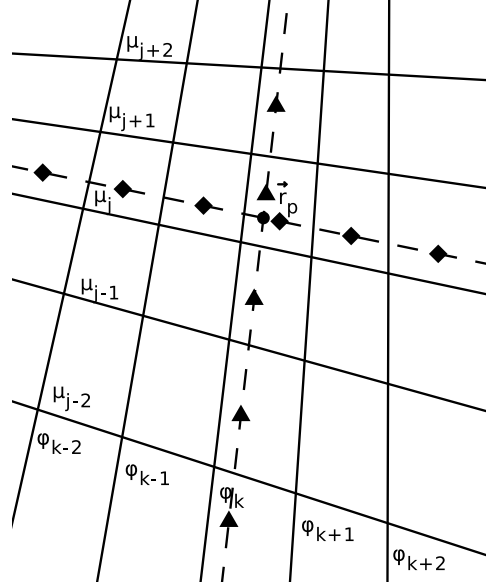
Fig. 5. Gaussian ray nearest neighbors (front view: t_n direction not shown).

of each beam at the source

$$g_{j'}(\vec{r}_p) = \frac{\left(\mu_{j'+1} - \mu_{j'}\right)}{\sqrt{2\pi w_{j'}^2}} \, exp\left(-\frac{d_{j'}^2}{2w_{j'}^2}\right) , \tag{38}$$

$$g_{k'}(\vec{r}_p) = \frac{\left(sin(\mu_{j'+1}) - sin(\mu_{j'})\right)\left(\varphi_{k'+1} - \varphi_{k'}\right)}{\sqrt{2\pi w_{k'}^2}} \, exp\left(-\frac{d_{k'}^2}{2w_{k'}^2}\right) , \tag{39}$$

where $w_{j'}$ and $w_{k'}$ are the half-widths of the Gaussian beam (from the cell center to one edge) in the μ and φ directions; and $d_{j'}^2$ and $d_{k'}^2$ are the distance in the μ and φ directions from the Gaussian beam center to the eigenray target. Unlike the Červený , GRAB, and BELLHOP models, which use the ray paths to describe the center of each beam, this new model aligns the ray paths with the edges of the Gaussian beam (full-width at half maximum).

Distance terms in the μ direction are calculated using the following pattern

$$L = 2 \, w_j \, \frac{\delta\mu}{\Delta\mu_j} , \tag{40}$$

$$d_j = L - w_j , \tag{41}$$

$$d_{j-1} = L - w_{j-1} , \tag{42}$$

$$d_{j-2} = L + 2w_{j-1} + w_{j-2} , \tag{43}$$

$$d_{j+1} = L - 2w_j - w_{j+1} \,, \tag{44}$$

$$d_{j+2} = L - 2w_j - w_{j+1} - w_{j+2} \tag{45}$$

where $\delta\mu$ is the eigenray offset in depression/elevation angle; $\Delta\mu$ is the depression/elevation width of this beam at the source; w_j is the width of beam j; and all widths have been interpolated to the time $t_n + \delta t$. More distant cells can be supported by adding additional $2w$ terms to Eqs. (43) and (45). The pattern in the azimuthal direction is similar.

GRAB[2] models the frequency dependent component of the beamwidth by giving each beam a minimum width

$$w'_j(f) = max\,(w_j, 2\pi\lambda) \,, \tag{46}$$

where λ is the wavelength of the signal being modeled; w_j is the cell width of beam j, and $w'_j(f)$ is the adjusted width of beam j. The λ term can be interpreted as the amount of evanescent spreading that GRAB expects beams to project into neighboring areas. In GRAB, Gaussian beams are overlapped by 50% to reduce fluctuations in the vicinity of the mid-point between rays.[13] The number of Gaussian profiles is effectively twice the number of ray paths.

The new algorithm treats beam width broadening as a convolution between a frequency dependent Gaussian propagation spread and a second Gaussian that represents the spatial spreading created by the sampling of the wavefront.

$$(w'_j(f))^2 = (2w_j)^2 + (2\pi\lambda)^2 \,. \tag{47}$$

It manages the 50% overlap by multiplying the cell width term by two. Treating the two spreading terms in this way avoids the sudden transitions inherent in taking a maximum value. Normalizing Eq. (38) by the combined effect of both spreading sources conserves energy across the wavefront.

Following the example of GRAB and BELLHOP, this new model uses Pedersen's challenging n[2] linear environment to provide an initial evaluation of propagation loss accuracy.[14]

$$c(z) = \frac{c_0}{\sqrt{1 + \dfrac{2g_0 z}{c_0}}} \,, \tag{48}$$

where $c(z)$ is speed of sound as a function of depth; z is depth (positive is down); c_0 is the speed of sound at the ocean surface (=1550.0 m/s); and g_0 is the sound speed gradient at the ocean surface (=1.2 s^{-1}). Note that this test uses the MKS version of the parameters defined in Jensen, Kuperman, et. al.[18] instead of Pedersen's original English units. As this test case is defined in "flat earth" Cartesian coordinates, a correction must be applied to Eq. (48) before it can be used by any model based on a spherical earth[15]

$$c(r) = \frac{r}{R}\,c(z) \,, \tag{49}$$

where r is the radial distance from the center of curvature; R is the radius of earth's curvature in this area of operations; $c(z)$ is the original sound speed; and $c(r)$ is the modified sound speed.

Fig. 6 plots the coherent propagation loss for this new model, as a function of range, for a source/receiver depth of 75 m, and a frequency of 2000 Hz. Target locations are analyzed between 500 and 1000 m to illustrate the behavior of the model near the edge of the shadow zone at 880 m. Fig. 6 also plots the corresponding results for the GRAB model and the Fast Field Program (FFP) wavenumber integration model.[16,17] Note that, in all regions, this implementation of FFP is consistent with an ideal wave equation solution except for the presence of some minor implementation jitter in the ranges above 880 m.

Prior to the shadow zone, all three models produce similar results. In the region beyond 840 m, this new approach and GRAB produce values that are similar to each other, but slightly higher than the theory. Results such as these lead us to believe that this new model can produce propagation loss values that are equivalent to standard benchmarks, even though the formulation of this new model makes significantly different assumptions.
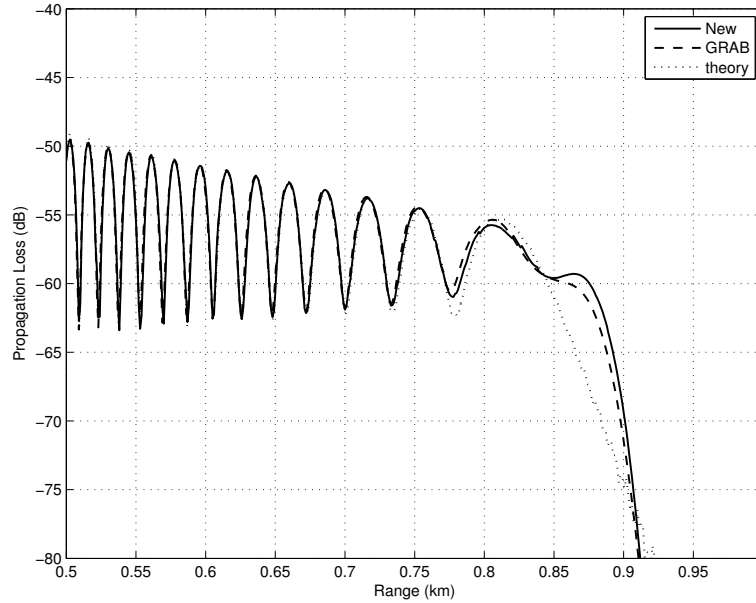

Fig. 6. Model comparisons at edge of shadow zone.

6. Summary

This paper has derived a new hybrid Gaussian beam model for computing propagation loss and eigenrays in a 3–D environment. The Gaussian beam components of this new approach leverage the concepts developed by Weinberg and Keenan for the GRAB model. However

unlike GRAB, which is 2–DxN , this new algorithm uses HARPO's latitude, longitude, and altitude concept as the basis for its 3–D propagation environment. Computing the propagation loss in the same coordinate system as the environmental parameters should provide this model with a computational speed advantage over other models. The derivation of this new approach requires the development of new equations for ray tracing, reflection, eigenray finding, and Gaussian beam propagation loss. Preliminary tests suggest that these changes have not had a negative impact on the accuracy of the model. However, more work is still required to verify and validate this accuracy and to evaluate the new model's computational efficiency.

Appendix

A. Derivation of the Ray Equations in Spherical/Time Coordinates

Ray theory decomposes acoustic waves into surfaces of constant travel time (t) from the source (Fig. A.1). The rays are a vector field that is normal to these surfaces at each point in space, and the route of these rays through the medium defines the direction of propagation. In the high frequency limit, spreading loss occurs as the energy of the wavefront is stretched over increasingly larger areas during propagation. Classic ray theory uses the change in distance between rays to model the spreading effects of wavefront propagation. The fundamental equations of ray theory are derived[18] by seeking solutions to the Helmholtz
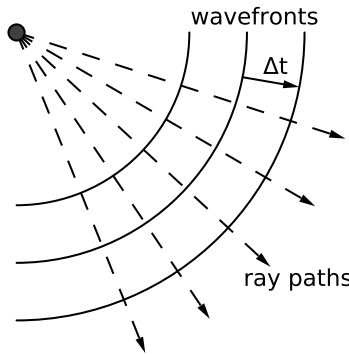

Fig. A.1. Acoustic ray geometry.

equation (A.1) in the form given by Eq. (A.2)

$$\nabla^2 p + \frac{\omega^2}{c^2(\vec{r})} p(\vec{r}) = -\delta(\vec{r} - \vec{r}_0) \tag{A.1}$$

$$p(\vec{r}) = e^{i\omega t(\vec{r})} \sum_{j=0}^{\infty} \frac{A_j(\vec{r})}{(i\omega)^j} . \tag{A.2}$$

Equating terms of like order in ω, yields the infinite sequence of equations given by Eqs. (A.3), (A.4), and (A.5)

$$O(\omega^2) : \left|\vec{\nabla}t\right|^2 = \frac{1}{c^2(\vec{r})} \,, \tag{A.3}$$

$$O(\omega) : 2\vec{\nabla}A_0 \cdot \vec{\nabla}t + (\nabla^2 t)A_0 = 0 \,, \tag{A.4}$$

$$O(\omega^{1-j}) : 2\vec{\nabla}A_j \cdot \vec{\nabla}t + (\nabla^2 t)A_j = -\nabla^2 A_{j-1} \qquad \text{for j=1,2,...} \tag{A.5}$$

where $\vec{r}$ is the position coordinate along a ray path; c is the speed of sound in water; A is the wavefront amplitude; and t is the travel time along the ray path. The eikonal equation (A.3) defines the relationship between the direction of propagation and the speed of sound in water. The first transport equation (A.4) relates the spreading loss of the acoustic field to the divergence in the propagation direction. The remaining transport equations (A.5) relate the spreading loss of the acoustic field to diffraction effects. Eqs. (A.3) and (A.4) are an exact solution of the wave equation in the geometric limit, that is, when the sound speed gradient along the direction of motion changes slowly compared to the acoustic wavelength. The accuracy starts to break down at lower frequencies where diffraction becomes a significant feature of acoustic propagation.

The analytic solution to the eikonal equation (A.3) is found[18] by relating $\vec{\nabla}t$ to $\hat{n}$, the direction of energy propagation along the ray paths

$$\hat{n} = \frac{d\vec{r}}{ds} = c\vec{\nabla}t \,. \tag{A.6}$$

This transforms the eikonal equation into a second order ordinary differential equation in terms of $\vec{r}$, c, and s

$$\frac{d}{ds}\left(\frac{1}{c}\frac{d\vec{r}}{ds}\right) = -\frac{1}{c^2}\vec{\nabla}c \,. \tag{A.7}$$

This can be reduced to a pair of simultaneous first order equations by introducing the temporary variable $\vec{\xi}$

$$\frac{d\vec{\xi}}{ds} = -\frac{1}{c^2}\vec{\nabla}c \,, \tag{A.8}$$

$$\frac{d\vec{r}}{ds} = c\vec{\xi} \,. \tag{A.9}$$

This set of equations can be solved using a series of arc length steps given initial conditions.[8,9] Equation (A.9) suggests that the temporary variable $\vec{\xi}$ is actually the direction of propagation scaled by the speed of sound, or equivalently, the wave number vector divided by the angular frequency

$$\vec{\xi} = \frac{\hat{n}}{c} = \frac{\vec{k}}{\omega} \,, \tag{A.10}$$

16   *S. M. Reilly, G. Potty*

where $\vec{k}$ is the acoustic wave number vector; and ω is the angular frequency of the acoustic source. This definition of $\vec{\xi}$ allows the system of equations represented by Eqs. (A.8) and (A.9) to be initialized with the position and steering angle for each ray path at the acoustic source. Note that the steering angle is defined using the depression/elevation (μ) and the azimuthal steering (φ) launch angles of each ray relative to the source. Marching the simultaneous first order equations (A.8) and (A.9) through steps in arc length then generates ray paths throughout the water column. The spreading loss of the wavefront at any point is calculated by measuring the spreading between adjacent rays. As adjacent rays have different travel times in this treatment, there is an implicit assumption that propagation loss is being calculated for a continuous ensonification at a single frequency.

To maintain the phase continuity of the wavefront, the change of variables defined in Eq. (A.11) is used to transform the ray equations into a function of travel time

$$\frac{d}{ds} = \frac{1}{c}\frac{d}{dt} , \tag{A.11}$$

$$\frac{d\vec{\xi}}{dt} = -\frac{1}{c}\vec{\nabla}c , \tag{A.12}$$

$$\frac{d\vec{r}}{dt} = c^2\vec{\xi} . \tag{A.13}$$

This form of the marching solution computes propagation as a series of steps in travel time and the phase coherence between rays is preserved at each step. This form of the ray equation represents a broadband impulse response of the environment in the high frequency limit. Note that although the ray paths represented by Eqs. (A.12) and (A.13) are independent of frequency, the loss along those paths will include the frequency dependent effects of seawater absorption and interface reflection.

This new approach uses the World Geodetic System 1984 (WGS–84)[19] reference ellipse to represent zero altitude worldwide (mean sea level). A spherical polar coordinate system is constructed within each area of operations, and its radius is set equal to the WGS–84 radius of curvature at the center of the area. This coordinate system is illustrated in Fig. B.2 where χ is latitude; ϕ is longitude; h is altitude above mean sea level; R is radius of earth's curvature for the area of operations; r is distance from the center of curvature (R+h); and θ is co-latitude ($90° - \chi$).

This model defines the average radius of curvature in the area of operations using a combination of WGS–84 radii in the latitude and longitude directions[7]

$$w^2 \equiv 1 - e^2 cos\chi , \tag{A.14}$$

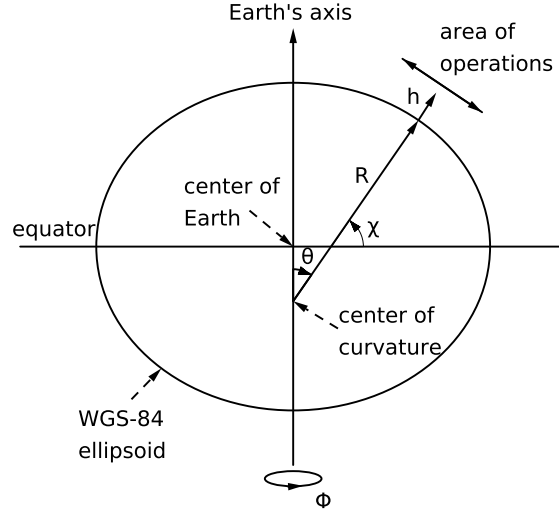$$R_\chi = \frac{a(1 - e^2)}{w^3} , \tag{A.15}$$

$$R_\phi = \frac{a}{w} , \tag{A.16}$$

Fig. B.2. Spherical earth coordinates.

$$R = \sqrt{R_\chi R_\phi} \tag{A.17}$$

where e is the WGS–84 elliptic eccentricity of earth $(8.1819190842622 \times 10^{-2})$; a is the WGS–84 equatorial radius of the earth (6378137.0 m); (R_χ, R_ϕ) are the radii of curvature in the latitude and longitude directions; and R is the average radius of curvature in area of operations.

From these definitions, all locations in the area of operations can be represented in terms of the spherical polar properties (r, θ, ϕ). The transformation of Eqs. (A.12) and (A.13) into this coordinate system uses the fact that the ray position only has radial components, while the ray direction has components in all three dimensions.[‡]

$$\vec{r}(t) = r(t)\hat{r}(t) , \tag{A.18}$$

$$\vec{\xi}(t) = \alpha(t)\hat{r}(t) + \beta(t)\hat{\theta}(t) + \gamma(t)\hat{\phi}(t) , \tag{A.19}$$

$$\frac{d\vec{r}}{dt} = \frac{dr}{dt}\hat{r} + r\frac{d\hat{r}}{dt} , \tag{A.20}$$

$$\frac{d\vec{\xi}}{dt} = \frac{d\alpha}{dt}\hat{r} + \alpha\frac{d\hat{r}}{dt} + \frac{d\beta}{dt}\hat{\theta} + \beta\frac{d\hat{\theta}}{dt} + \frac{d\gamma}{dt}\hat{\phi} + \gamma\frac{d\hat{\phi}}{dt} \tag{A.21}$$

where $\alpha(t)$, $\beta(t)$, and $\gamma(t)$ are the radial, co-latitude, and longitude components of the normalized ray direction. Note that the unit vectors $\hat{r}$, $\hat{\theta}$, and $\hat{\phi}$ in Eqs. (A.20) and (A.21)

[‡]This derivation uses arrows for vectors with magnitude and direction (such as $\vec{r}$), carets for unit length vectors (such as $\hat{r}$), and plain text for magnitude parameters (such as r).

18   *S. M. Reilly, G. Potty*

change as a function of r, θ, and ϕ. The impact of these derivatives can be understood by casting them into their Cartesian coordinate equivalents before applying the time derivative

$$\hat{r}(t) = sin\theta(t)\,cos\phi(t)\,\hat{i} + sin\theta(t)\,sin\phi(t)\,\hat{j} + cos\theta(t)\,\hat{k}\,, \tag{A.22}$$

$$\hat{\theta}(t) = cos\theta(t)\,cos\phi(t)\,\hat{i} + cos\theta(t)\,sin\phi(t)\,\hat{j} - sin\theta(t)\,\hat{k}\,, \tag{A.23}$$

$$\hat{\phi}(t) = -sin\phi(t)\,\hat{i} + cos\phi(t)\,\hat{j}\,. \tag{A.24}$$

The chain rule, when applied to Eqs. (A.22), (A.23), and (A.24) yields the following time derivatives in spherical coordinates

$$\frac{d\hat{r}}{dt} = \frac{d\theta}{dt}\hat{\theta} + sin\theta\frac{d\phi}{dt}\hat{\phi}\,, \tag{A.25}$$

$$\frac{d\hat{\theta}}{dt} = -\frac{d\theta}{dt}\hat{r} + cos\theta\frac{d\phi}{dt}\hat{\phi}\,, \tag{A.26}$$

$$\frac{d\hat{\phi}}{dt} = -sin\theta\frac{d\phi}{dt}\hat{r}\,. \tag{A.27}$$

Applying Eqs. (A.25) through (A.27) to Eqs. (A.20) and (A.21) transforms the ray tracing equations into spherical earth coordinates

$$\frac{d\vec{r}}{dt} = \frac{dr}{dt}\hat{r} + r\frac{d\theta}{dt}\hat{\theta} + rsin\theta\frac{d\phi}{dt}\hat{\phi}\,, \tag{A.28}$$

$$\frac{d\vec{\xi}}{dt} = \left[\frac{d\alpha}{dt} - \beta\frac{d\theta}{dt} + \gamma sin\theta\frac{d\phi}{dt}\right]\hat{r} + \left[\frac{d\beta}{dt} + \alpha\frac{d\theta}{dt} - \gamma cos\theta\frac{d\phi}{dt}\right]\hat{\theta} \\ + \left[\frac{d\gamma}{dt} + (\alpha sin\theta + \beta cos\theta)\frac{d\phi}{dt}\right]\hat{\phi}\,. \tag{A.29}$$

Matching terms for $\hat{r}$, $\hat{\theta}$, and $\hat{\phi}$ yields a system of six first-order, scalar differential equations

$$\frac{dr}{dt} = c^2\alpha\,, \tag{A.30}$$

$$r\frac{d\theta}{dt} = c^2\beta\,, \tag{A.31}$$

$$rsin\theta\frac{d\phi}{dt} = c^2\gamma\,, \tag{A.32}$$

$$\frac{d\alpha}{dt} - \beta\frac{d\theta}{dt} - \gamma sin\theta\frac{d\phi}{dt} = -\frac{1}{c}\frac{dc}{dr}\,, \tag{A.33}$$

$$\frac{d\beta}{dt} + \alpha \frac{d\theta}{dt} - \gamma cos\theta \frac{d\phi}{dt} = -\frac{1}{cr} \frac{dc}{d\theta} \, , \tag{A.34}$$

$$\frac{d\gamma}{dt} + (\alpha sin\theta + \beta cos\theta) \frac{d\phi}{dt} = -\frac{1}{cr sin\theta} \frac{dc}{d\phi} \, . \tag{A.35}$$

When Eqs. (A.30) though (A.32) are plugged into Eqs. (A.33) though (A.35), the system is reduced to a state where all of the coordinate derivatives appear only once

$$\frac{dr}{dt} = c^2 \alpha \, , \tag{A.36}$$

$$\frac{d\theta}{dt} = \frac{c^2 \beta}{r} \, , \tag{A.37}$$

$$\frac{d\phi}{dt} = \frac{c^2 \gamma}{r sin\theta} \, , \tag{A.38}$$

$$\frac{d\alpha}{dt} = -\frac{1}{c} \frac{dc}{dr} + \frac{c^2}{r} \left(\beta 2 + \gamma^2 \right) \, , \tag{A.39}$$

$$\frac{d\beta}{dt} = -\frac{1}{cr} \frac{dc}{d\theta} - \frac{c^2}{r} \left(\alpha\beta + \gamma^2 cot\theta \right) \, . \tag{A.40}$$

$$\frac{d\gamma}{dt} = -\frac{1}{cr sin\theta} \frac{dc}{d\phi} - \frac{c^2 \gamma}{r} \left(\alpha + \beta cot\theta \right) \, . \tag{A.41}$$

These are the ray equations in spherical/time coordinates.

Acknowledgments

References

1. P. A. Baxley, H. Bucker, M. B. Porter, Comparison of Beam Tracing Algorithms, *Proceedings of the Fifth European Conference on Underwater Acoustics (ECUA)* 2000.
2. H. Weinberg, R. E. Keenan, Gaussian ray bundles for modeling high-frequency propagation loss under shallow-water conditions, *J. Acoust. Soc. Amer.* **100** (1996) 1421.

20   *S. M. Reilly, G. Potty*

3. Software Requirements Specification/Software Design Description and Software Test Description for the Oceanographic and Atmospheric Master Library Navy Standard Comprehensive Acoustic System Simulation Model Version 4.2A, *Naval Meteorology and Oceanography Command Report OAML-SRS-SDD-STD-83D* (2008).
4. V. Červený , M. M. Popov, and I. Pšencík, Computation of wave fields in inhomogeneous media - Gaussian beam approach, *Geophys. J. R. Astron. Soc.* **70** (1982) 109.
5. M. B. Porter, Y. C. Liu, Finite Element Ray Tracing, *International Conference on Theoretical and Computational Acoustics (ICTCA)* Volume 2 (1994) 947.
6. M. B. Porter, H. P. Bucker, Gaussian beam tracing for computing ocean acoustic fields, *J. Acoust. Soc. Amer.* **93** (1987) 1349.
7. R. M. Jones, J.P. Riley, T.M. Georges, HARPO: A Versatile Three-Dimensional Hamiltonian Ray-Tracing Program for Acoustics Waves in an Ocean with Irregular Bottom, *National Oceanic and Atmospheric Administration (NOAA) Report*, (1986).
8. Yakowitz and Szidarovszky, An Introduction to Numerical Computation (Macmillan Publishing, New York, 1986) pp. 306-311.
9. W. Press, S. Teukolsky, W. Vetterling, B. Flannery, Numerical Recipes in C (Cambridge University Press, New York, 1992), pp 747-752.
10. ETOPO1v2 Global Gridded 2-minute Database, National Geophysical Data Center, National Oceanic and Atmospheric Administration, U.S. Dept. of Commerce, http://www.ngdc.noaa.gov/mgg/global/ETOPO1.html.
11. F. Sturm, S. Ivansson, Y. M. Jiang, N. R. Chapman, Numerical investigation of out-of-plane sound propagation in a shallow water experiment, *J. Acoust. Soc. Amer.* **124** (2008) pp. 341-346.
12. R. W. Sinnott, Virtues of the Haversine, *Sky and Telescope* **68** (1984) 159.
13. H. Weinberg, R. E. Keenan, Gaussian ray bundles for modeling high-frequency propagation loss under shallow-water conditions, NUWC-NPT Technical Report 10,568 (1996).
14. M. A. Pedersen, D. F. Gordon, Normal-Mode and Ray Theory Applied to Underwater Acoustic conditions of Extreme Downward Refraction, *J. Acoust. Soc. Amer.* **51** (1972) 323.
15. C. L. Pekeris, Accuracy of the Earth-Flattening Approximation in the Theory of Microwave Propagation, *Phys. Rev.* **70** (1943).
16. F. R. DiNapoli, R. L. Deavenport, Theoretical and numerical Green's function field solution in a plane multilayered medium, *J. Acoust. Soc. Amer.* **67** (1980).
17. L. M. Brekhovskikh, Waves in Layered Media (Academic Press Inc., New York, 1980), 2nd Edition, Section 54.
18. F. B. Jensen, W. A. Kuperman, M. B. Porter, and H. Schmidt, Computational Ocean Acoustics (American Institute of Physics Press, New York, 1994) pp. 150-153.
19. WGS 84 Implementation Manual, Version 2.4, *European Organization for the Safety of Air Navigation, and the Institute of Geodesy and Navigation*, (1998).